



A significant improvement of the processing and electric properties of CeO₂ co-doped with Ca and Sm by mechanosynthesis

A. Moure*, C. Moure, J. Tartaj

Instituto de Cerámica y Vidrio, CSIC, C/Kelsen, 5, 28049 Madrid, Spain

ARTICLE INFO

Article history:

Received 18 March 2011
Received in revised form 23 May 2011
Accepted 10 July 2011
Available online 3 September 2011

Keywords:

Solid Oxide Fuel Cell
Electrolyte
Ceria
Mechanosynthesis

ABSTRACT

High energetic milling of the corresponding oxides and carbonates mixture was employed to obtain highly dense ceramics with Ce_{0.80}Sm_{0.20-x}Ca_xO_{1.9} (x = 0, 0.02) compositions at low sintering temperature. After 17 h of milling, the samarium and calcium have entered in the ceria fluorite-type structure, indicating that the mechanosynthesis of the material has occurred. Densities in the order of 97–98% were obtained at temperatures as low as 1250–1300 °C in a single thermal treatment. Besides, the addition of Ca is shown as a clear aid to sinter high-density ceramics with improved grain size for the increase of the ionic conductivity. The high homogeneity of the mixture allows Ca not only to partially incorporate to the structure, but also to react to the glassy siliceous phase located at the grain boundary. This effective cleaning process, together with the additional grain growth promoted by Ca doping, increases the grain boundary conductivity, and thus, the total conductivity of the ceramics. The influence of the microstructure on the electrical properties of the ceramics is discussed.

© 2011 Elsevier B.V. All rights reserved.

1. Introduction

Solid Oxide Fuel Cells (SOFC) are electrochemical devices that directly convert chemical energy into electrical energy and, on contrary to batteries, they work continuously consuming a fuel (generally hydrogen) of some sort [1]. In these devices, the electrolyte is constituted by a polycrystalline oxide material with high oxygen conductivity that determines the efficiency of the cell. A common electrolyte material is the so-called yttrium stabilized zirconia (YSZ), which is a composition of ZrO₂ optimized by doping with 8 mol% Y₂O₃. However, this material has a limit in its performance because it works well only at temperatures in the order of 900–1000 °C due to its relatively low ionic conductivity (<0.1 S cm⁻¹) [2]. To reduce the working conditions to intermediate temperatures (500–900 °C), alternative materials are currently tested, such as CeO₂ doped with alkaline-earth or mainly with rare earth oxides [3,4]. The doping cations as Ca²⁺, Gd³⁺ or Sm³⁺ are incorporated in the ceria structure and, due to the difference in the valence state among these cations with Ce⁴⁺, oxygen vacancies are created, increasing the ionic conductivity of the materials. It has been shown that the substitution of cerium by calcium (among the alkaline-earth elements) and samarium (among the rare-earth elements) produces the best results among the alkaline-earth and rare-earth elements, respectively. This is due to the similar ionic radius of the

host and the doping cations, which minimizes the elastic deformation of the structure [3,5].

A major problem related with the use of ceria is the high sintering temperature needed to obtain ceramics with densities higher than 97%, as required for electrolyte applications in SOFC devices. Typical sintering temperatures are in the order of 1500–1600 °C when the precursors are obtained by classical solid state reactions, preventing the possibility of cosintering with other components of the cell. Different processing routes have been tested to reduce the sintering temperature, including the use of transition metals as sintering aids [6], with the drawback of the increase of electronic conductivity. Two problems are associated with this issue. One is the possible lack of homogeneity in the microstructure at such processing temperatures. The other one is the reduction from Ce⁴⁺ to Ce³⁺, which is more important at increasing temperatures [3]. When this phenomenon occurs, a change in the volume of the material is produced, which can damage the mechanical properties of the ceramic body. The Ce reduction also introduces an electronic component to the total conductivity of the electrolyte [4] that drastically reduces the cell performance [7].

Another problem associated with the use of ceria as electrolyte material is the difference between bulk and grain boundary resistivity. The latter is much higher than the former, limiting in this way the total ionic conductivity of the ceramic. The presence of Si in the precursors of ceria is a common feature within these materials [8]. This silica-rich glassy phase forms a continuous network that blocks the ionic carriers, diminishing the grain boundary conductivity in ceria. Based on experiments employing highly pure materials (with

* Corresponding author.

E-mail address: alberto.moure@icv.csic.es (A. Moure).

Si contents lower than 50 ppm), other authors attribute this behavior to an intrinsic contribution from space charge layer regions [9]. Guo and Waser reported that in fact both intrinsic and extrinsic phenomena contribute to the reduction of the grain boundary conductivity [10]. The use of highly pure materials is difficult and expensive, thus alternatives are needed to reduce the grain boundary resistivity due to these extrinsic contributions caused by Si. It has been reported that the scavenging of the siliceous phase by the addition of small quantities of alkaline-earth elements (as Mg [11] and Ca [12,13]) is an adequate and cheaper way to clean the grain boundary and to decrease its resistivity.

$\text{Ce}_{0.8}\text{Sm}_{0.2-x}\text{Ca}_x\text{O}_{1.9}$ compositions were chosen in this study because Sm has been proved to be the dopant that produces the highest conductivity, and also decreases the reducibility of ceria [4]. Ca in small quantities has shown to be a good dopant to decrease the grain boundary resistivity [12]. It reacts with the Si-rich impurities and cleans the grain boundary. In this work, high energetic milling in planetary mill has been employed to process the ceramics. This method allows the sintering temperature to be reduced due to the high reactivity of the obtained precursors, as well as a better incorporation of Sm and Ca to the structure to create the oxygen vacancies. The prolonged milling produces a constant and homogenous mixture of the components, allowing that a part of calcium can react with impurities and the rest incorporate to the ceria structure avoiding the calcination step at high temperatures needed to decompose CaCO_3 . Although the mechanical activation or the mechanosynthesis is a widely used route in ceramics processing [14], few works have been reported in the processing of materials for electrolytes in SOFC applications [15–17]. The effect of the milling on the materials processing and in the sintering behavior of the ceramics is shown. Measurements of the conductivity by impedance spectroscopy were carried out in order to study the influence of the microstructure and the calcium addition on the conductivity of the ceramics.

2. Experimental procedure

Ceramic precursors of $\text{Ce}_{0.8}\text{Sm}_{0.2-x}\text{Ca}_x\text{O}_{1.9}$ ($x=0, 0.02$) compositions were obtained by high energetic milling. The stoichiometric quantities of CeO_2 , Sm_2O_3 and CaCO_3 necessary to obtain 10 g of the ceramic precursors were placed in a WC pot with seven balls (also WC), 2 cm diameter, 437 g mass, for a relation of masses 45/1. Milling was carried out with a Pulverizette 5 model Fritsch planetary mill operating at 250 rpm.

Evolution with time of the milled precursors was monitored by Bragg–Brentano X-ray diffraction (XRD) with a Bruker AXS D8 Advance diffractometer. $\text{Cu K}\alpha$ radiation ($\lambda = 1.5418 \text{ \AA}$) and a $5 \times 10^{-2} \text{ deg s}^{-1}$ scan rate were used. The crystal size (t) was obtained from the XRD data using the Scherrer formula: $t = 0.9\lambda / B \cos \theta_B$, where λ is the wavelength used, B is the full width at half maximum of the diffraction peak and θ_B is the Bragg angle [18]. X-ray fluorescence (XRF) technique was used (spectrometer Phillips model PW-2424) to determine the possible contamination of the milled precursors. For the analysis, a sample of 0.3 g in fusion with 5.5 g of $\text{Li}_2\text{B}_4\text{O}_7$ was prepared. Powder precursors were characterized with a Zeiss Microscope (model DSM 950, Oberkochem, Germany).

The powder obtained after prolonged milling was studied by Differential Thermal Analysis (DTA)–Thermogravimetric (TG) techniques. A thermoanalyzer Netzsch, model STA-409 was used up to 1200°C , in an alumina crucible with a heating rate of $10^\circ\text{C min}^{-1}$ was employed.

Approximately 0.7 g amounts of the as-milled powders were uniaxially pressed in pellets with 0.8 mm diameter at 100 MPa and then isostatically pressed at 200 MPa. The shrinkage behavior was

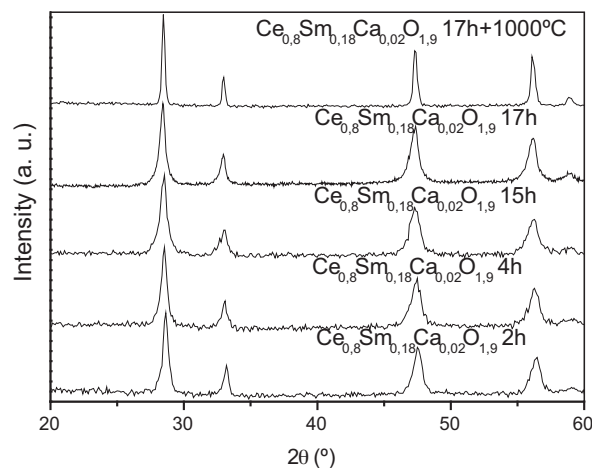


Fig. 1. XRD patterns of the stoichiometric mixture of Ce_2O_3 , Sm_2O_3 and CaCO_3 precursor of $\text{Ce}_{0.8}\text{Sm}_{0.2-x}\text{Ca}_x\text{O}_{1.9}$ ($x=0, 0.02$) ceramics, after different milling times and crystallized at 1000°C after milling during 17 h.

studied using a dilatometer Netzsch Gerätebau (model 402 EP, Selb-Bayern Germany) up to 1600°C with a heating and cooling rate of 5°C min^{-1} .

The pellets were then sintered in air at conditions detailed later and based on the dilatometric results, and then characterized by XRD at the same conditions as for the precursors. Density of the ceramics was measured by Archimede's method in distilled water at room temperature. After polishing and thermal etching, the microstructures of the sintered samples were examined by scanning electron microscopy in a Zeiss Microscope (model DSM 950, Oberkochem, Germany). Impedance was measured using a LF Impedance analyser (model HP-4294A, Hewlett-Packard) on disk-shaped pellets Ag electrodes (Dupont) calcined at 700°C –1 h, at frequencies from 100 Hz to 10 MHz.

3. Results and discussion

Fig. 1 shows the evolution with time of the oxides and carbonate mixture for $\text{Ce}_{0.8}\text{Sm}_{0.18}\text{Ca}_{0.02}\text{O}_{1.9}$ milled up to 17 h, together with the mixture milled for 17 h and then thermally treated at 1000°C when a good crystallization of the materials has been obtained, as the narrowness of the peaks indicates. The composition without Ca shows similar results to those shown in **Fig. 1**. An increase in the width of the diffraction peaks is observed at increasing milling time, indicating a decrease of the particle size. Due to the similarity in the positions of the peaks of CeO_2 (JCPDS 34-0394) and Sm_2O_3 (JCPDS 15-0813), it is difficult to follow the evolution with the milling of each oxide. However, a slight shift of the main diffraction peak to lower angles is observed as the milling time increases, from 28.64° after 2 h to 28.4° after 17 h of milling. The peak position is maintained after a thermal treatment at 1000°C , and agrees well with that corresponding to the previously reported for $\text{Ce}_{0.8}\text{Sm}_{0.2}\text{O}_{1.9}$ (JCPDS 75-0160). This could be an indication that at increasing milling time the Sm and Ca enter in the CeO_2 structure, until they would be totally incorporated after 15 and 17 h. This statement cannot be totally confirmed from these results. However, it can at least be stated that the high energetic milling is improving the conditions at which Sm and Ca can be introduced in the structure, as the results of the sintering ceramics study will show below. In comparison with solid state method, lower temperatures are needed to achieve the incorporation and to process the ceramics by the use of mechanosynthesis.

Fig. 2 shows the DTA–TG curves of the mixture of both compositions after 17 h of milling. There are practically no differences

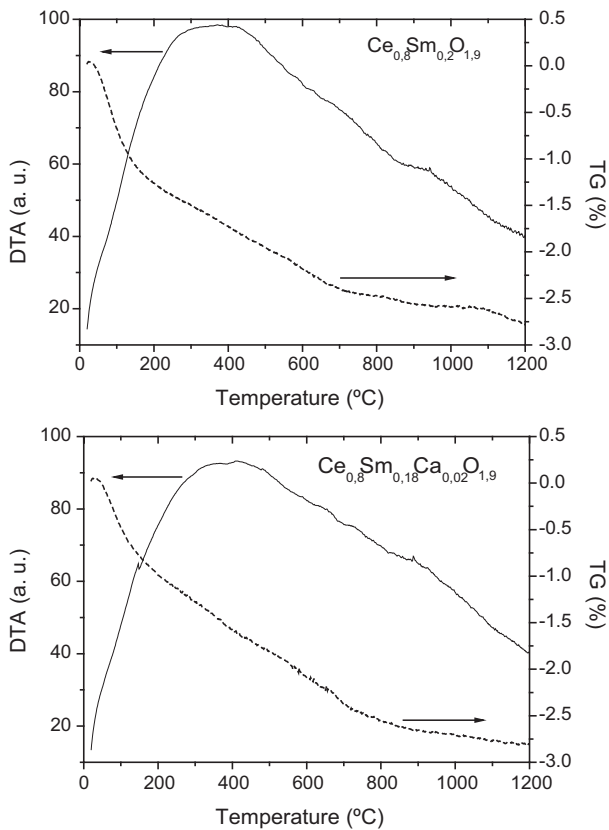


Fig. 2. DTA and TG curves of the stoichiometric mixture of Ce_2O_3 , Sm_2O_3 and CaCO_3 after 17 h of milling.

between the materials with and without calcium. The DTA curves do not show any significant variations that could be attributed to incorporation of Sm, suggesting that it is totally incorporated in the structure after milling. The TG curve shows the same weight loss for the Ca doped and no-doped materials. Due to the presence of CaCO_3 among the precursors in the $\text{Ce}_{0.8}\text{Sm}_{0.18}\text{Ca}_{0.02}\text{O}_{1.9}$, a difference of 0.5% of weight loss is expected between both compositions. This is not observed in Fig. 2. This means that during milling the CaCO_3 has decomposed and the calcium has probably mostly reacted and entered in the CeO_2 structure. This is necessary to achieve the mechanosynthesis of the $\text{Ce}_{0.8}\text{Sm}_{0.2-x}\text{Ca}_x\text{O}_{1.9}$ after 17 h of milling. This is a significant advantage of mechanosynthesis with respect to the solid state reaction method for the incorporation of Ca in the material. When this route is used, Ca is only incorporated after the decomposition of the initial CaCO_3 at temperatures higher than 800°C . It limits the calcination step to high temperatures, giving place to large particles that makes difficult the subsequent sintering process. The calcination step is avoided by the mechanosynthesis obtained during milling.

Fig. 3 shows the micrographs obtained by SEM of the powders after milling during 17 h. Agglomerates in the order of $1\text{--}2.5\ \mu\text{m}$ can be observed. They are built up by smaller crystallites. Although they cannot be clearly identified in Fig. 3, their sizes are in the nanometric range. This is in good agreement with the sizes in the order of 20 nm calculated by Scherrer formula from the XRD patterns shown in Fig. 1. This crystallite size is similar to that found in materials processed by mechanosynthesis, also for SOFC applications [17]. These characteristics have an influence on the sintering of the ceramics, as it will be shown below.

Fig. 4 shows the shrinkage behavior of the green pellets for $\text{Ce}_{0.8}\text{Sm}_{0.20}\text{O}_{1.9}$ and $\text{Ce}_{0.8}\text{Sm}_{0.18}\text{Ca}_{0.02}\text{O}_{1.9}$ compositions prepared from mechanosynthesized precursors. For the Ca-doped material,

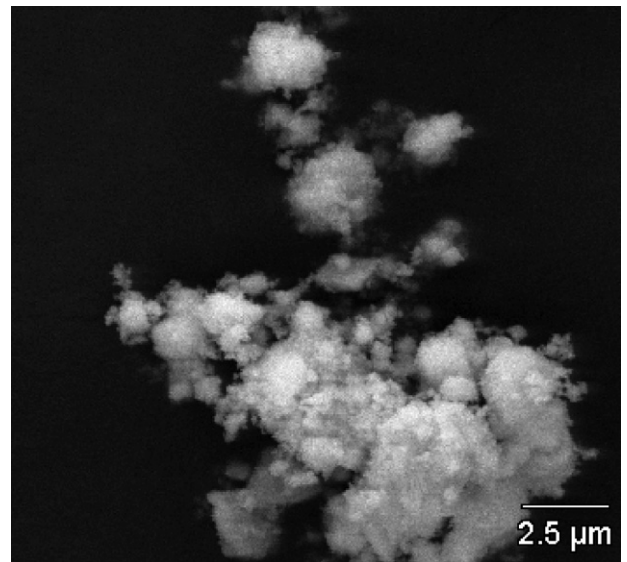


Fig. 3. SEM micrographs of precursor powders of $\text{Ce}_{0.8}\text{Sm}_{0.18}\text{Ca}_{0.02}\text{O}_{1.9}$ ceramics after 17 h of milling at 5000 amplification.

a continuous contraction is observed in the whole temperature range, but only a peak is observed in the shrinkage rate curve, centered at 1180°C approximately. From 1400°C , the contraction is much slower, indicating that the maximum densification has been achieved. The curves are different for the $\text{Ce}_{0.8}\text{Sm}_{0.20}\text{O}_{1.9}$ composition. Two peaks in the shrinkage rate are observed, centered at 1320 and 1530°C , approximately. These different behaviors can lead to strong differences in the microstructures of the ceramics.

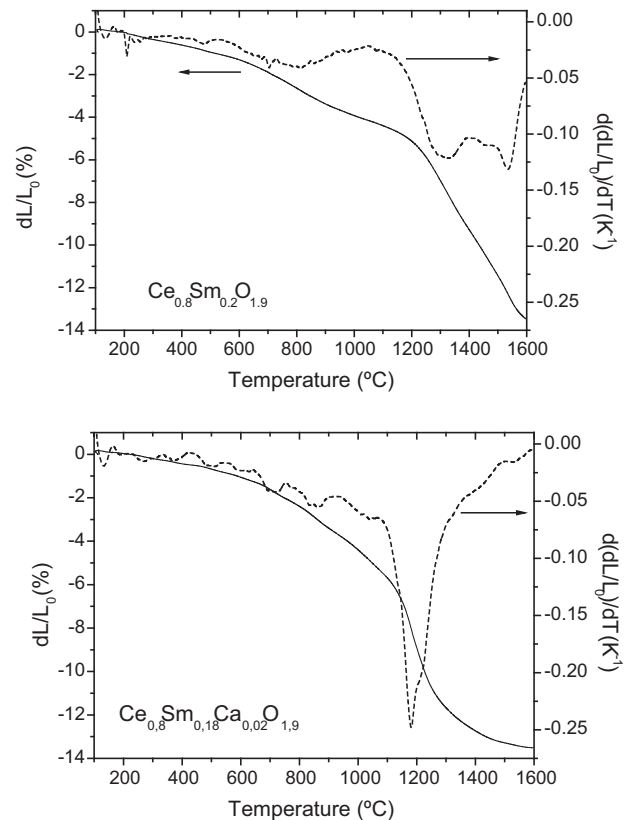


Fig. 4. Shrinkage and shrinkage rate of green pellets of the $\text{Ce}_{0.8}\text{Sm}_{0.20}\text{O}_{1.9}$ and $\text{Ce}_{0.8}\text{Sm}_{0.18}\text{Ca}_{0.02}\text{O}_{1.9}$ compositions.

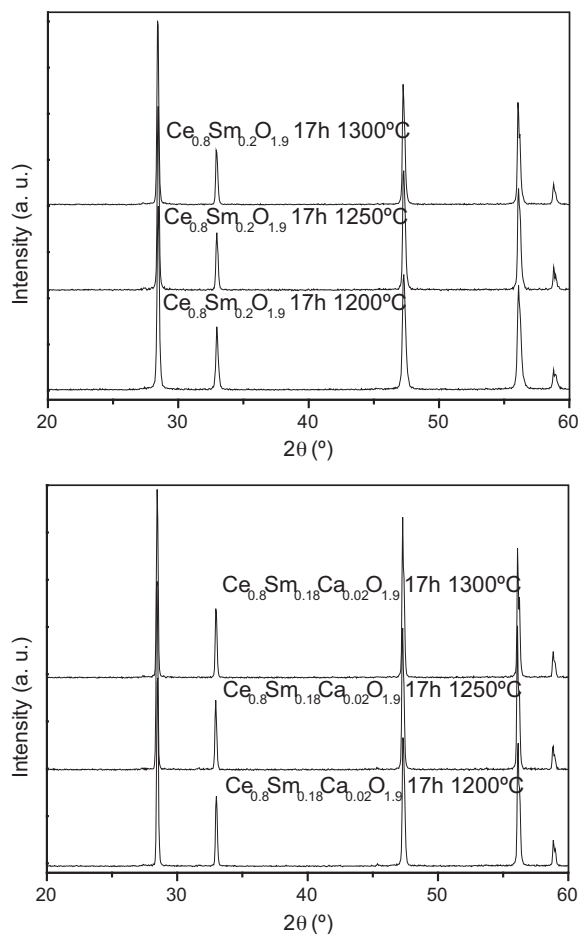


Fig. 5. XRD patterns of $\text{Ce}_{0.8}\text{Sm}_{0.2}\text{O}_{1.9}$ and $\text{Ce}_{0.8}\text{Sm}_{0.18}\text{Ca}_{0.02}\text{O}_{1.9}$ ceramics sintered from precursors obtained by mechanosynthesis after 17 h of milling.

The shrinkage behavior gives information of the conditions at which the ceramics can be sintered. It must be remarked that the use of mechanical assisted methods by high energetic milling allows the processing of the ceria ceramics to be carried out in a single thermal treatment, i.e. the step corresponding to the solid solution formation at intermediate temperatures is avoided, for the first time to the authors' best knowledge. Three different sintering temperatures (1200, 1250, 1300 °C, determined by the Ca-doped shrinkage curve) during 2 and 4 h have been checked. Fig. 5 shows the XRD patterns for both compositions. The peaks positions agree well with that of the pattern corresponding to $\text{Ce}_{0.8}\text{Sm}_{0.2}\text{O}_{1.9}$ (JCPDS 15-0813). This means that single phase ceramics with Sm and Ca incorporated to the structure of CeO_2 are obtained by sintering of the mechanosynthesized precursors in a single thermal treatment.

The theoretical density of $\text{Ce}_{0.80}\text{Sm}_{0.20}\text{O}_{1.9}$ (7.148 g cm^{-3}) has been taken from the data of the JCPDS 75-0160 file. For the $\text{Ce}_{0.80}\text{Sm}_{0.18}\text{Ca}_{0.02}\text{O}_{1.9}$ composition, it was calculated from the molecular weight and the cell volume calculated from the XRD data shown in Fig. 5. In this case, the theoretical density has been taken as 7.017 g cm^{-3} . Values of relative density in the order of 97–98% were obtained at 1250–1300 °C in the case of Ca doped ceramics, for 2 h of sintering. Longer times (4 h) are needed in the case of the materials without calcium to achieve improved results according to the Archimedes's measurement. The density is higher for the Ca doped material at lower temperatures and shorter times, indicating that calcium is an aid for the densification of the ceramics. It allows both temperatures and time sintering to be decreased. The times

are slightly decreased with respect to similar compositions (with Gd doping, without Ca) prepared by mechanosynthesis [16], where high densities (>98%) were achieved only after long sintering time (15 h), also at 1300 °C.

It is remarkable the high density achieved at relatively low temperatures by mechanosynthesis in comparison with the classical solid state reaction method, where temperatures higher than 1500–1600 °C are needed to attain a highly dense ceramics of Sm-doped ceria [19–21]. Recently, Ayawanna has reported that in Sm-doped ceria processed by classical solid state reaction, the relative density of the ceramics sintered at 1400 °C during 5 h is only 91%, approximately [22]. Other processing methods have also been successfully used to lower the sintering temperature in Sm-doped ceria. Densities varying from 96 to 99% were achieved at temperatures between 1200 and 1400 °C by different routes, as carbonate precipitation, coprecipitation, autocombustion, spray pyrolysis or sol-gel [23–27]. An added advantage of the mechanosynthesis is the higher simplicity of the processing. All the mentioned methods based on chemical routes need several steps of calcination and drying in the processing of the precursors. This is the first report of a processing route for ceria doped with samarium ceramics in a single thermal treatment from the initial oxides mixtures to the final dense ceramics with such relevant results. Even the drying process used by W.S. Jung et al. [16] is avoided, because milling is carried out here without any liquid media. This shows the advantage of using the mechanosynthesis in the processing of Ca, Sm co-doped ceria. As Ca and Sm are introduced in the structure during milling, calcination step at high temperatures, mandatory to decompose CaCO_3 in the classical solid state method, is avoided. The highly reactive powder obtained allows to carry out the processing in a single thermal step and at lowered temperature.

Fig. 6 shows the micrographs of polished and thermally etched ceramics with and without Ca sintered at 1250 and 1300 °C during 2 h, to better compare the influence of Ca in the microstructure. A clear difference is observed in the ceramics depending on the composition. The results pointed out in the measurement of the density by Archimedes method are confirmed in the micrographs, which explains well the cause of the higher porosity of the ceramics without Ca. It appears mainly in the regions of open porosity. It can be due to the certain degree of agglomeration that has been observed elsewhere in mechanosynthesized precursors [28]. At increasing the sintering temperature to 1300 °C, a more amount of voids among the larger particles are closed. The microstructure evolves to a close porosity. The remaining pores are those of the regions that have not totally closed those voids, and they are still relatively large (1–1.5 μm) in comparison with the grain size. At both temperatures, the regions inside the agglomerates show a good densification (insets in Fig. 6a and b). This microstructure explains the shrinkage rate curve, where two peaks appeared. The one at lower temperature corresponds to the close of the porosity inside agglomerates, while the second peak at higher temperatures is due to the densification among agglomerates. At the sintering temperatures employed in this work, this second process is not totally activated, leading to the relatively high porosity observed in Fig. 6 for $\text{Ce}_{0.8}\text{Sm}_{0.2}\text{O}_{1.9}$ ceramics.

The densification of the ceramics with Ca is clearly improved, and an advanced close porosity is observed at 1250 °C after 2 h of sintering, with pores being smaller than the grain size. By increasing the sintering temperature to 1300 °C, the pores are quite isolated and remain in a small amount. The ceramics of $\text{Ce}_{0.80}\text{Sm}_{0.18}\text{Ca}_{0.02}\text{O}_{1.9}$ sintered at 1250 °C and mainly at 1300 °C present the adequate microstructure for SOFC electrolytes applications. The addition of small quantities of Ca has an influence on the sintering temperatures and also on the sintering times. The regions inside the agglomerates and at the zones where the porosity is closed are quite well densified in $\text{Ce}_{0.80}\text{Sm}_{0.20}\text{O}_{1.9}$ ceramics,

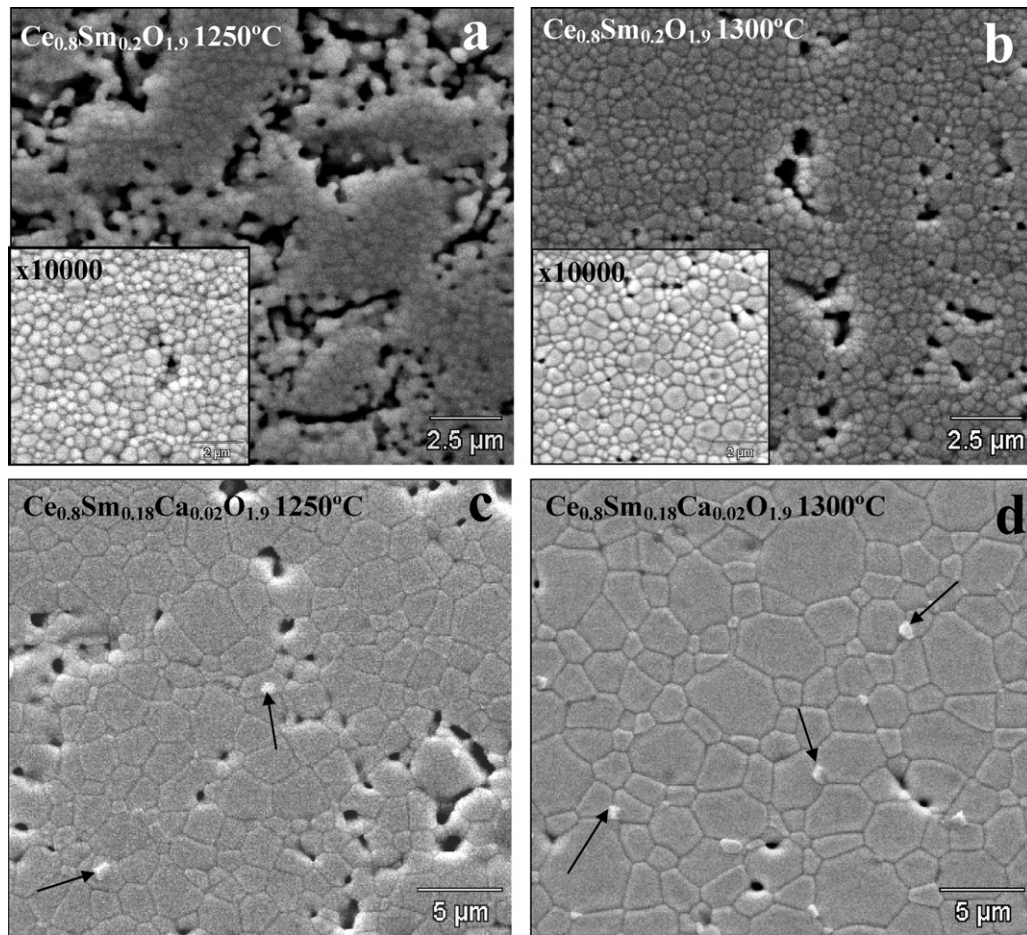


Fig. 6. SEM micrographs of $\text{Ce}_{0.8}\text{Sm}_{0.2}\text{O}_{1.9}$ and $\text{Ce}_{0.8}\text{Sm}_{0.18}\text{Ca}_{0.02}\text{O}_{1.9}$ ceramics sintered at 1250 and 1300 °C from mechanosynthesized precursors milled during 17 h. Note the change of scale from $\text{Ce}_{0.8}\text{Sm}_{0.2}\text{O}_{1.9}$ ($\times 5000$ magnification) to $\text{Ce}_{0.8}\text{Sm}_{0.18}\text{Ca}_{0.02}\text{O}_{1.9}$ ($\times 3000$ magnification). Insets: $\text{Ce}_{0.8}\text{Sm}_{0.2}\text{O}_{1.9}$ ceramics sintered at 1250 and 1300 °C with a $\times 10,000$ magnification.

without any abnormal grain growth and a good continuity for the conductivity. It seems that at longer sintering time the voids could close, favored by the reduced grain size that promotes the mass transport through grain boundaries. Calcium is accelerating the processes, producing a higher densification at lower temperatures and times. This is shown thus as a first advantage for the addition of small amounts of Ca to Sm-doped ceria ceramics.

The presence of Ca in the composition has also an influence on the grain size of the ceramics. The $\text{Ce}_{0.80}\text{Sm}_{0.18}\text{Ca}_{0.02}\text{O}_{1.9}$ composition has much larger grain size than the $\text{Ce}_{0.80}\text{Sm}_{0.20}\text{O}_{1.9}$ one. Even sintering at 1250 °C, when Ca is introduced, produces larger grains than sintering at 1300 °C. The ceramics without Ca have submicron sizes, being only the largest grains after sintering at 1300 °C of the order of 1 μm . The microstructures of the $\text{Ce}_{0.80}\text{Sm}_{0.20}\text{O}_{1.9}$ ceramics sintered at 1250 and 1300 °C are similar between them, as it occurs for the $\text{Ce}_{0.80}\text{Sm}_{0.18}\text{Ca}_{0.02}\text{O}_{1.9}$ ceramics. This indicates that differences of 50 °C in the sintering temperature have a stronger effect on the densification than on the grain growth. In fact, the main difference is only observed for the largest grains between the Ca-doped ceramics. They are in the order of 2–3 μm for the ceramics sintered at 1250 °C, and 4–5 μm for those sintered at 1300 °C. The comparison of the grain growth can be only carried out with routes that are alternative to classical solid state method, because they use sintering temperatures in the order of those employed in this work. Thus, grain size of the $\text{Ce}_{0.80}\text{Sm}_{0.20}\text{O}_{1.9}$ ceramics shown in Fig. 6 is in the order of those reported in samples sintered at 1250 °C from precursors prepared by glycine–nitrate process [29].

Ramesh et al. also reported grain sizes similar to that shown in Fig. 6d for $\text{Ce}_{0.78}\text{Sm}_{0.2}\text{Ca}_{0.02}\text{O}_{2-\delta}$ ceramics, prepared by sintering at 1300 °C from powders obtained by sol–gel [27]. This last comparison shows that the increase in grain size due to Ca doping is not exclusive of the mechanosynthesis process, but is associated with the presence of Ca, and it was also pointed in Gd-doped ceria [30]. The presence of W in the powder was detected by XRF analysis, but in a much less quantity than Ca (0.12 and 0.74 wt%, respectively, taking into account that W is almost 5 times heavier than Ca). The comparison with Ramesh's work shows that the only presence of Ca is increasing the grain size, and W can be ruled out as an aid for sintering. Even the reaction of Ca with Si located at the grain boundaries can have an influence. Some authors have previously reported [31] that in the system calcia–silica, a liquid phase is formed at sintering temperatures higher than 1436 °C, based on its phase diagram. The sintering temperatures used here are lower (up to 1300 °C), but the presence of Ce and Sm could have an influence and form a transient eutectic to produce a liquid-assisted sintering. In any case, this is a second advantage of the doping with calcium. The increase in the grain size diminishes the grain boundary density per volume, reducing the portion of conduction through them. This is an advantage in SOFC applications as it produces an increase in ionic conductivity, although it must be pointed that it could also lead to the worsening of the strength, which can become important due to the stress gradient under operating conditions [32,33].

Similarly to the finding by Cho et al. [13], only a small part of Ca enters in the structure at this doping content. EDS analysis were

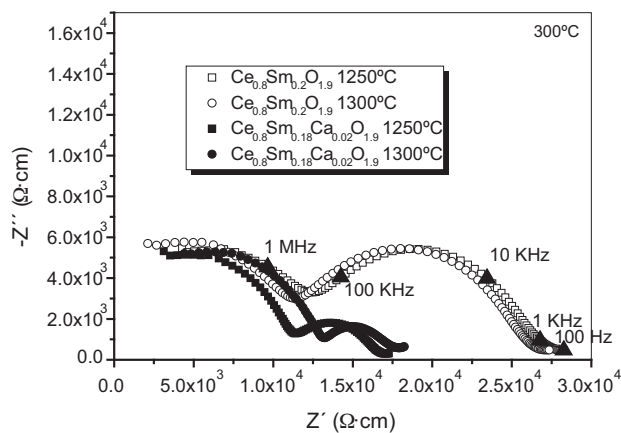


Fig. 7. Impedance spectra of ceramics with $\text{Ce}_{0.8}\text{Sm}_{0.2}\text{O}_{1.9}$ and $\text{Ce}_{0.8}\text{Sm}_{0.18}\text{Ca}_{0.02}\text{O}_{1.9}$ composition at temperatures close to 300°C .

carried out at individual grains. Some of them did not show any trace of Ca, while in others it was detected, although in a smaller quantity than the expected, taken into account the small amounts of Ca and the limit in the detection of the technique. In any case, Ca is quite diluted or even not present in some of the grains. Besides the part of the calcium that introduces in the structure, other part has placed out of the grains, despite the fact that the quantities used in this work are far from the limit of solubility of Ca in ceria (20 mol%) [34]. It is so because Ca gives place to an additional phase marked with arrows in Fig. 6d. Analysis by EDS, which results are not detailed in this work, shows that this phase is composed by Ca, Ce and Sm (which can also come from the adjacent ceramic matrix). It also contains traces of W, coming from the milling media, and that overlaps the signal from Si, which cannot be quantified but it is known to be present, as approximately 600 ppm of Si were detected by XRF analysis in the ceria raw material.

These microstructures have an effect on the conductivity of the ceramics. Fig. 7 shows the impedance spectra at approximately 300°C corresponding to the doped ceria ceramics shown in Fig. 6. This temperature was chosen for a better comparison of the arcs corresponding to bulk resistivity (at high frequencies) to those of grain boundary resistivity (at low frequencies). The ceramics without calcium present higher total resistivity than the Ca-doped ones. It is also significant the differences in the relative size of the grain boundary arcs with respect to the bulk ones. The latter are much smaller than the former in the $\text{Ce}_{0.80}\text{Sm}_{0.20}\text{O}_{1.9}$ ceramics, but they are much more similar, or even the grain boundary arcs being smaller, in the $\text{Ce}_{0.8}\text{Sm}_{0.18}\text{Ca}_{0.02}\text{O}_{1.9}$ composition. This clearly shows that the doping with calcium has an important influence on the grain boundary conduction.

This is reflected in the Arrhenius plots of the bulk, grain boundary and total conductivity of the ceramics shown in Fig. 8. The data were obtained at each temperature from impedance spectra similar to those shown in Fig. 7. The bulk conductivity is quite similar for both compositions. This is related with the relatively small amount of Ca that enters in the grain structure, as EDS analysis has shown. Thus, the grains of the $\text{Ce}_{0.8}\text{Sm}_{0.18}\text{Ca}_{0.02}\text{O}_{1.9}$ and $\text{Ce}_{0.8}\text{Sm}_{0.20}\text{O}_{1.9}$ ceramics have a close composition, and differences in the bulk conductivity are not observed. On the contrary, the grain boundary conductivity, as well as the total conductivity is higher for the calcium doped ceramics. To remark this point, the grain boundary blocking factor α_{GB} was calculated as defined in [24] by the ratio $r_{\text{GB}}/r_{\text{tot}}$, where r_{GB} is the grain boundary resistance and r_{tot} is the total resistance. The values at 200 and 300°C are shown in Table 1. The blocking factor is lower than 0.5 (that is, the total resistance is mainly governed by bulk conductivity at those temperatures) at both temperatures only for the $\text{Ce}_{0.8}\text{Sm}_{0.18}\text{Ca}_{0.02}\text{O}_{1.9}$ ceramics, and

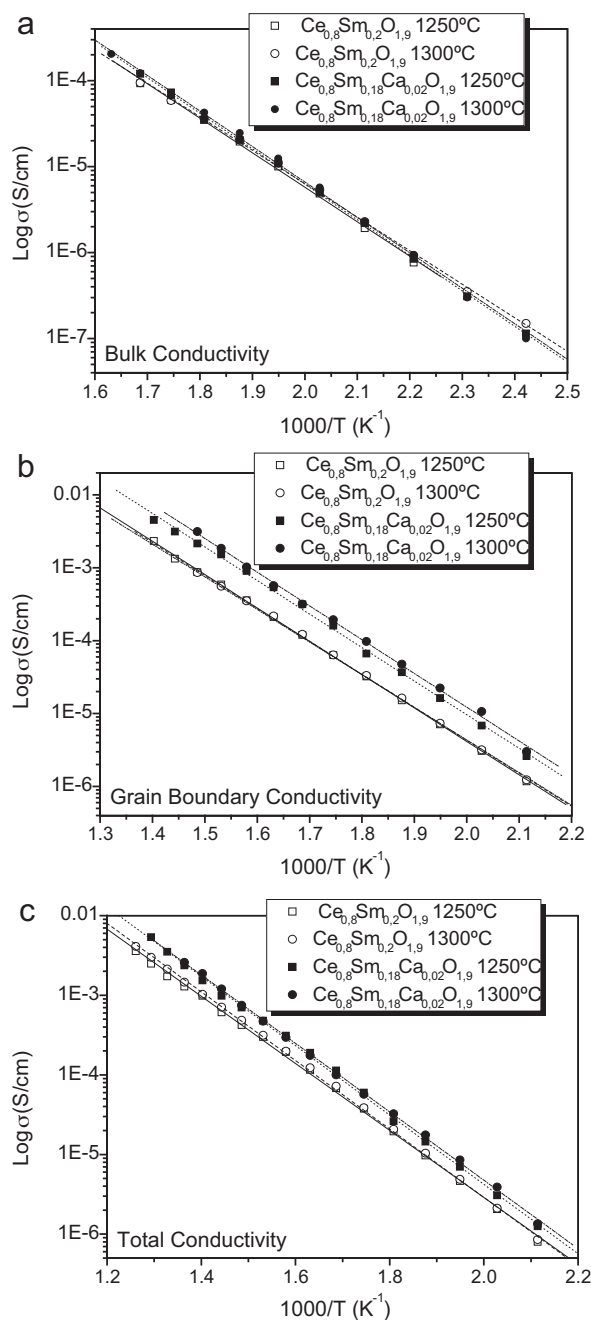


Fig. 8. Arrhenius plots of the (a) bulk, (b) grain boundary and (c) total conductivity of $\text{Ce}_{0.8}\text{Sm}_{0.20}\text{O}_{1.9}$ and $\text{Ce}_{0.8}\text{Sm}_{0.18}\text{Ca}_{0.02}\text{O}_{1.9}$ ceramics.

has almost double values at 300°C in the $\text{Ce}_{0.8}\text{Sm}_{0.20}\text{O}_{1.9}$ ceramics. The results show lower blocking factors than those previously reported in references [24,35] in ceramics without Ca. The effect of the doping with Ca on the improvement of the grain boundary and total conductivity is clear. As it was stated above, the presence of W in the particles marked by an arrow in Fig. 6d makes difficult the detection of Si. However, by analogy with what was previously reported in ceria ceramics doped with Gd and Ca obtained by coprecipitation [36] and other methods [13], and in view of the results of the conductivity measurements, it can be deduced that Ca has also reacted with the Si placed in the grain boundaries, to produce a different phase that moves to the triple points. At these positions, the presence of these secondary phases has a smaller influence on the conductivity than a Si phase along the grain boundaries, as they are scarce and quite diluted along the ceramic. The same

Table 1

Activation energy and pre-exponential factor of the bulk, grain boundary and total conductivity; grain boundary blocking factor at 200 and 300 °C.

	E_a^{Bulk} (eV)	σ_0^{Bulk} (S cm ⁻¹)	E_a^{GB} (eV)	σ_0^{GB} (S cm ⁻¹)	E_a^{Total} (eV)	σ_0^{Total} (S cm ⁻¹)	α_{GB} (200 °C)	α_{GB} (300 °C)
Ce _{0.8} Sm _{0.2} O _{1.9}								
1250 °C-2 h	0.81	6.83	0.91	8.77	0.84	6.64	0.68	0.59
1300 °C-2 h	0.78	6.18	0.89	8.26	0.85	7.05	0.69	0.61
Ce _{0.8} Sm _{0.2-x} Ca _x O _{1.9}								
1250 °C-2 h	0.82	7.05	0.94	10.11	0.87	7.69	0.48	0.37
1300 °C-2 h	0.82	7.08	0.90	9.61	0.84	7.36	0.45	0.29

can be said about the presence of small amounts of contamination. This, together with the increase of the grain size and the associated decrease of the grain boundary density, leads to the improvement of the grain boundary conductivity. The third advantage of the addition of the calcium can be stated: the capacity of cleaning the grain boundaries from Si phases, diminishing their resistivity.

The activation energies corresponding to the bulk, grain boundary and total conductivities are shown in Table 1. They are in the order of those previously reported in similar compositions of ceria doped with Sm, and with Sm and Ca [27,35,37]. However, the activation energy of the conductivity could vary from 0.6 to almost 1.0 eV depending on the preparation method [38]. The values for both compositions and sintering temperatures are quite similar, being slightly higher for grain boundary than for bulk. The higher conductivity for Ce_{0.8}Sm_{0.18}Ca_{0.02}O_{1.9} ceramics and also through grain boundaries despite their higher activation energy is due to the fact that conductivity is also a function of the pre-exponential factor [3], according to the expression.

$$\sigma = \sigma_0 \cdot \exp\left(-\frac{E_a}{kT}\right) \quad (1)$$

The values of σ_0 are also higher for the Ca-doped ceramics and grain boundaries (Table 1), confirming this tendency.

The values of the total resistivity at 300 °C for the Ce_{0.8}Sm_{0.18}Ca_{0.02}O_{1.9} ceramics sintered at 1300 °C ($1.76 \times 10^4 \Omega \text{ cm}$), corresponding to a conductivity of $5.68 \times 10^{-5} \text{ S cm}^{-1}$) can be compared to that found by Esposito et al. [24] ($R \sim 2 \times 10^4 \Omega \text{ cm}$) in ceramics sintered at higher temperatures (1400 °C, without Ca), and those reported by Ramesh et al. [27] ($4.09 \times 10^{-5} \text{ S cm}^{-1}$) in Ce_{0.78}Sm_{0.2}Ca_{0.02}O_{2- δ} ceramics sintered at 1300 °C, with a relative density of 96%. These results show the efficiency of the processing by mechanosynthesis of Ca, Sm co-doped ceria ceramics as candidates to be used as electrolytes in SOFC applications.

4. Conclusions

The mechanosynthesis of Ce_{0.8}Sm_{0.2-x}Ca_xO_{1.9} ($x=0, 0.02$) compositions has been achieved by high energetic milling in a planetary mill after 17 h. The high reactivity of the precursors obtained by this route allows to process the Ce_{0.8}Sm_{0.2-x}Ca_xO_{1.9} ceramics for the first time in a single thermal step where densification and grain growth takes place. A reduction of the sintering temperatures is achieved with respect to the classical solid state method, with densities higher than 98% at relatively low temperatures (1250–1300 °C) for Ca-doped ceramics.

The addition of calcium has three major advantages: decreases the sintering temperature with improved densification; increases the grain size; and reacts with Si phases on the grain boundaries to form a new phase with Ca and Si composition that moves to the triple points, where it has a minor influence on the grain boundary conductivity. All these advantages result in an important improvement of the grain boundary conductivity, and, as a consequence, an increase of the total conductivity with respect to the non-Ca-doped Ce_{0.80}Sm_{0.20}O_{1.9} ceramics. The combination of mechanosynthesis and doping with calcium improves the processing and properties

of Ce_{0.80}Sm_{0.20}O_{1.9} ceramics for applications as electrolytes in SOFC applications.

Acknowledgments

This work was supported by Spain PROFIT CIT-120000-2007-50 and MICINN MAT2008-06785-C02-02-E. Dr. A. Moure is indebted to the CSIC (MICINN) of Spain for the “Junta de Ampliación de Estudios” contract (Ref JAEDOC087). The authors are grateful for the technical support provided by Mr. Fernando Resano.

References

- [1] G. Hoogers, in: G. Hoogers (Ed.), Fuel Cell Technology Handbook, CRC Press, Boca Raton, FL, 2003, pp. 1-1-1-5.
- [2] E.C. Subbarao, H.S. Maiti, Solid State Ionics 11 (4) (1984) 317–338.
- [3] H. Inaba, H. Tagawa, Solid State Ionics 83 (1996) 1–16.
- [4] M. Mogensen, N.M. Sammes, G.A. Tompsett, Solid State Ionics 129 (2000) 63–94.
- [5] H.L. Tuller, J. Phys. Chem. Solids 55 (12) (1994) 1393–1404.
- [6] C. Kleinlogel, L.J. Gauckler, Adv. Mater. 13 (14) (2001) 1081–1085.
- [7] B.C.H. Steele, Solid State Ionics 134 (2000) 3–20.
- [8] R. Gerhardt, A.S. Nowick, M.E. Mochele, I. Dumler, J. Am. Ceram. Soc. 69 (1986) 647–651.
- [9] B. Li, X. Wei, W. Pan, Int. J. Hydrogen Energy 35 (2010) 3018–3022.
- [10] X. Guo, R. Waser, Prog. Mater. Sci. 51 (2006) 151–210.
- [11] Y.H. Cho, P.S. Cho, G. Aucherlonie, D.K. Kim, J.-H. Lee, D.-Y. Kim, H.-M. Park, J. Drennan, Acta Mater. 55 (2007) 4807–4815.
- [12] A. Moure, J. Tartaj, C. Moure, J. Eur. Ceram. Soc. 29 (2009) 2559–2565.
- [13] P.S. Cho, S.B. Lee, Y.H. Cho, D.-Y. Kim, H.-M. Park, J.-H. Lee, J. Power Sources 183 (2008) 518–523.
- [14] L.B. Kong, T.S. Zhang, J. Ma, F. Boey, Prog. Mater. Sci. 53 (2) (2008) 207–322.
- [15] K. Maca, J. Cihlar, K. Castkova, O. Zmeskal, H. Hadraba, J. Eur. Ceram. Soc. 27 (2007) 4345–4348.
- [16] W.-S. Jung, H.-S. Park, Y.J. Kang, D.-H. Yoon, Ceram. Int. 36 (2010) 371–374.
- [17] A. Moure, A. Castro, J. Tartaj, C. Moure, J. Power Sources 188 (2009) 489–497.
- [18] B.D. Cullity, in: M.A. Reading (Ed.), Elements of X-ray Diffraction. Addison-Wesley Series in Metallurgy and Materials, Addison-Wesley, Massachusetts, 1967.
- [19] Z. Zhan, T.-L. Wen, H. Tu, Z.-Y. Lu, J. Electrochem. Soc. 148 (5) (2001) A427–A432.
- [20] T. Ishida, F. Iguchi, K. Sato, T. Hashida, H. Yugami, Solid State Ionics 176 (2005) 2417–2421.
- [21] S. Omar, E.D. Wachsman, J.C. Nino, Solid State Ionics 178 (2008) 1890–1897.
- [22] J. Ayawanna, D. Wattanasiriwech, S. Wattanasiriwech, P. Aungkavattana, Solid State Ionics 180 (2009) 1388–1394.
- [23] Y. Wang, T. Mori, J.-G. Li, Y. Yajima, J. Drennan, J. Eur. Ceram. Soc. 26 (2006) 417–422.
- [24] V. Esposito, E. Traversa, J. Am. Ceram. Soc. 91 (4) (2008) 1037–1051.
- [25] R.V. Mangalaraja, S. Ananthakumar, A. Schachtsiek, M. López, C.P. Camurri, R.E. Avila, Mater. Sci. Eng. A 527 (2010) 3645–3650.
- [26] H.C. Jang, D.S. Jung, J.H. Kim, Y.C. Kang, Y.H. Cho, J.-H. Lee, Ceram. Int. 36 (2010) 465–471.
- [27] S. Ramesh, V.P. Kumar, P. Kistaiah, C.V. Reddy, Solid State Ionics 181 (2010) 86–91.
- [28] A. Moure, A. Castro, J. Galy, C. Moure, J. Tartaj, J. Am. Ceram. Soc. 93 (2010) 3206–3213.
- [29] D. Yan, X. Liu, X. Bai, L. Pei, M. Zheng, C. Zhu, D. Wang, W. Su, J. Power Sources 195 (2010) 6486–6490.
- [30] J.D. Nicholas, L.C. De Jonghe, Solid State Ionics 178 (2007) 1187–1194.
- [31] J.A. Lane, J.L. Neff, G.M. Christie, Solid State Ionics 177 (2006) 1911–1915.
- [32] A. Atkinson, Solid State Ionics 95 (1997) 249–258.
- [33] A. Atkinson, T.M.G.M. Ramos, Solid State Ionics 129 (2000) 259–269.
- [34] M. Yamashita, K. Kameyama, S. Yabe, S. Yoshida, Y. Fujishiro, T. Kawai, T. Sato, J. Mater. Sci. 37 (2002) 683–687.
- [35] C. Sánchez-Bautista, A.J. Dos Santos-García, J. Peña-Martínez, J. Canales-Vázquez, Bol. Soc. Esp. Ceram. 49 (1) (2010) 7–14.
- [36] A. Moure, J. Tartaj, C. Moure, Mater. Lett. 65 (2011) 89–91.
- [37] M. Dudek, J. Eur. Ceram. Soc. 28 (2008) 965–971.
- [38] D. Ding, B. Liu, M. Gong, X. Liu, C. Xia, Electrochim. Acta 55 (2010) 4529–4535.